Carbon 114 (2017) 8–14

Contents lists available at ScienceDirect

Carbon

journal homepage: www.elsevier.com/locate/carbon

Preparation of monodispersed sulfur nanoparticles-partly reduced graphene oxide-polydopamine composite for superior performance lithium-sulfur battery

Yiyong Zhang, Kun Li, Jingxin Huang, Yunhui Wang, Yueying Peng, He Li, Jing Wang, Jinbao Zhao*

State Key Laboratory of Physical Chemistry of Solid Surfaces, Collaborative Innovation Center of Chemistry for Energy Materials, College of Chemistry and Chemical Engineering, Xiamen University, Xiamen 361005, PR China

ARTICLE INFO

Article history:
Received 9 September 2016
Received in revised form
24 November 2016
Accepted 29 November 2016
Available online 30 November 2016

ABSTRACT

Lithium-sulfur battery has received extensive attention because of its high energy density, but its practical application has been limited by several problems such as short cycle life and low efficiency. In this study, we prepare monodispersed sulfur nanoparticles (S NPs) on partially reduced graphene oxide (S-prGO) during reduction of graphene oxide by spray method. The S-prGO composite is then recombined with polydopamine (PDA) to get the S-prGO-PDA composite. The S-prGO-PDA composite exhibits great cycling stability, coulombic efficiency and capacity retention. When charge-discharge at current density of 200 mA g^{-1}, the specific capacity is 1122 mAh g^{-1} at the first discharge and 647 mAh g^{-1} after 100 cycles, with stable coulombic efficiency of 98%.

1. Introduction

Growing market demand in consumer electronics, energy storage system and electric vehicles has triggered significant researches on advanced power source. The lithium-sulfur (Li-S) battery is one of the most promising candidates due to its high theoretical specific energy density (2600 Wh kg^{-1}), low cost and high natural abundance of sulfur [1–5]. However, in the case of sulfur cathodes, achieving longevity of cycling in Li-S batteries is still hindered by the following factors. One is the electrical insulating nature of elemental sulfur and its discharge products which lead to the low utilization of active sulfur. Also, diffusion and shuttle of the polysulfide intermediates will make a lot of sulfur species lost in the electrolyte and deposit on the lithium anode [6].

To solve these obstacles, various kinds of carbon materials are normally used to prepare carbon-sulfur (C-S) composites as the active cathode material, such as active C-S composites [1,2,7], mesoporous C-S composites [8,9], graphene-sulfur composites [10–15] and carbon nanotubes-sulfur composites [16–22]. Though the carbon materials can effectively improve the electron conductivity of sulfur cathode, the interactions between non-polar carbon and polar polysulfide intermediates is weak. As a result, the physical barriers provided by sequestration and adsorption in carbon materials can only slow down the polysulfide intermediates diffusion in a short term, because the polysulfide intermediates are driven by the electric field in the electrolyte. Furthermore, the weak interaction can cause the detachment and separation of lithium sulfides (Li_2S_x, $1 < x < 2$), the full-discharged products, from the carbon matrix which will be a factor to cause irreversible active mass loss and electrical contact isolation [23,24]. Hence the stronger physical or chemical interaction of sulfur and its discharge products to the carbon host is fundamentally essential to eliminate the polysulfide shuttling and the capacity decay. Thus, Li et al. [25] proposed that we should the rational design and synthesis of various hollow micro-/nanostructures with controlled shapes, tailored shell structures and designed chemical compositions for advanced Li-S batteries in the future. A lot of researchers exploited oxygen-containing functional groups on graphene oxide to fix the sulfur and demonstrated that oxygen-containing functional groups on graphene oxide [12,13,26,27] are conducive to immobilize polysulfides. The *Ab initio* calculations based on the adsorption of S [13] or S_3 [12] clusters indicated that both epoxy (C═O) and hydroxyl (—OH) groups can enhance the binding of S to the C—C bonds due to the induced charge transfer. And to mitigate this problem,

* Corresponding author.
E-mail address: jbzhao@xmu.edu.cn (J. Zhao).

http://dx.doi.org/10.1016/j.carbon.2016.11.079
0008-6223/

Wang et al. [28] reported a facile approach towards high-performance sulfur-carbon cathodes by covalently stabilizing the sulfur and its discharge products on amino-functionalized reduced graphene oxide which enabled to get stable capacity retention of 80% for 350 cycles with high capacities and excellent high-rate response up to 4 C. Li et al. [29] also reported a 'pie' structured electrode, which provided an excellent balance between gravimetric and areal energy densities. Combining lotus root-like multichannel carbon nanofibers 'filling' and amino-functionalized graphene'crust', the free-standing paper electrode (S mass loading: 3.6 mg cm^{-2}) delivered high specific capacity of 1314 mAh g^{-1} (4.7 mAh cm^{-2}) at 0.1 C (0.6 mA cm^{-2}) accompanied with good cycling stability.

In this study, we have developed a facile and one-step method to prepare monodispersed S NPs on partly reduced graphene oxide with different reduction levels followed by coating with PDA to prepare S-prGO-PDA composite. In such structure, the nanosized S NPs will lead to better sulfur utilization, and the larger specific surface area will lead to smaller effective current density and faster discharging kinetics. It has been demonstrated that the trade-off between high specific capacity and high rate performance may be resolved in ultrasmall S NPs [30]. Besides, the oxygen-containing functional groups on graphene oxide and the amino of PDA are conducive to immobilize polysulphides. By adjusting the degree of the graphene oxide reduction, the conductivity can be enhanced and simultaneously oxygen-contained functions are retained. The PDA is further coated on the S NPs to confine the sulfur species on the cathode. The results show that the electrochemical performance is critically dependent on the reduction level of graphene oxide and the nanosize effect on Li-S batteries is obvious. Importantly, we have demonstrated that a certain reduction degree of graphene oxide synergistic PDA can stabilize polysulfides and their discharge products, and can also provide electronic conductivity. Therefore, the improved cycle performance, coulombic efficiency and capacity retention rate of Li-S batteries are exhibited.

2. Experiment

2.1. Material synthesis

Firstly, the graphene oxide (GO) was synthesized by modified Hummers method. Then, the GO was dispersed in deionized water by ultrasonic dispersion method, getting the GO suspension with concentration of 4 mg mL^{-1}. According to the designed proportion, 1.8 g sulfur (S) and 0.5 g reductant ascorbic acid (VC) were added to the ethylene glycol or *n*-octanol solvent of 200 mL, followed by heating to 160 °C or 180 °C in an oil bath pan and maintaining the constant temperature. The corresponding amount of GO suspension was sprayed into the above isothermal solvent containing S by using a spray gun at the sample rate of 4 mL min^{-1} with the mass ratio of S and GO at 3: 1 and the carrier gas of nitrogen. The flow rate of carrier gas was 100 mL min^{-1}. After spraying, the mixture continued keeping at the constant temperature (160 °C or 180 °C) for 0.5 h and then cooled naturally, which was washed by absolute ethanol and deionized water and dried by a freeze-dryer to get finally composite material S-prGO (noted as S-prGO-160, S-prGO-VC-160, and S-prGO-VC-180 according to the synthesis temperature and whether to add VC, respectively.). In order to further improve the S-capturing ability of the composite, the S-prGO composites were recombined with PDA, and the synthetic method is described as following: 0.5 g S-prGO composite material was added into 100 mL deionized water with magnetic stirring for 1 h, then 40 mg tris(hydroxymethyl) aminomethane buffer (Tris/HCl) was joined to adjust the pH value with magnetic stirring for another 1 h, followed in sequence by adding 60 mg of dopamine hydrochloride (DA/HCl) for aggregation, mixing by the magnetic stirrer overnight, taking out the dispersion liquid by suction filtration and vacuum drying at 60 °C. Finally the S-prGO-PDA composite material was obtained.

2.2. Characterization

The morphologies of as-prepared materials were characterized by using a scanning electron microscope (SEM, HITACHI S-4800) equipped with energy dispersive X-ray spectroscopy (EDX) for elemental analysis. Transmission electron microscopy (TEM) images was tested on JEM-2100 (JEOL, Japan) at 200 kV. The XRD patterns of the S-prGO and S-prGO-PDA composites were recorded by the Philips X'pert Pro Super X-ray diffract meter and Cu Kα radiation. The laser Raman spectra were recorded at the resolution of 1 cm^{-1} in back scattering (180°) configuration using 532 nm excitation. X-ray photoelectron spectroscopy (XPS) was conducted on PHI Quantum 2000 Scanning ESCA Microprobe.

2.3. Electrochemical measurements

The slurry with composition of 70 wt% S-prGO-PDA active materials, 20 wt% carbon black and 10 wt% polyvinylidene fluorides (PVDF) dissolved in *N*-methyl pyrrolidone (NMP), was casted onto an aluminum foil and dried under vacuum at 60 °C overnight to prepare the working electrodes. The areal sulfur loading was about 1 mg cm^{-2}. The CR2016-type coin cells were assembled using the prepared electrodes and lithium metal in an argon-filled glove box. The volume of the electrolyte in a coin cell was 60 μL. The electrolyte was formed by adding lithium bis(trifluoromethanesulfonyl)imide (LiTFSI, 1 M) salt and lithium nitrate ($LiNO_3$, 1 wt%) into the mixture of 1,3-dioxolane (DOL) and 1,2-dimethoxyethane (DME) at the volume ratio of 1:1. The galvanostatic charge-discharge experiments were measured at different current densities between 1.8 and 2.6 V (vs. Li^+/Li) using the CT2001A cell test instrument (XINWEI Electronic Co.). The electrochemical impedance spectroscopy (EIS) of the S-prGO-PDA electrodes was recorded by the autolab PGSTAT 101 cell test instrument in the frequency range of 10 mHz−100 kHz, using two-electrode coin cells with Li metal as the counter electrode. All of the electrochemical tests were performed at room temperature.

3. Results and discussion

The synthesis process of monodispersed S NPs on partly reduced graphene oxide (S-prGO) is shown in Fig. 1. As we can see, in a typical synthesis, the reduction of GO and the recombination of the S-prGO composite are achieved at the same time. Because of the mild reduction conditions, the reduction degree of prGO is not completely, which will be proved by the following facts. The GO dispersion liquid is added into the ethylene glycol solution containing S and ascorbic acid (VC) at a certain temperature by spraying method. The S-prGO is prepared during the reduction process of GO. By carefully adjusting preparation conditions such as temperature and the amount of VC, the S-prGO with different reduction levels is prepared, and then the S-prGO is composited with PDA to obtain the composite material noted as S-prGO-PDA.

Apparent photograph of the obtained S-prGO composites are shown in Fig. 2a. It is easy to see that the colour of the S-prGO composites gradually deepened for GO, S-prGO-160, S-prGO-VC-160 and S-prGO-VC-180, successively. This means more uniformly mixed S with prGO as adding VC and increasing the temperature. Simultaneously, it also indirectly indicate that the reduction degree of graphene oxide gradually increases. In order to analyze the morphology of the prepared composites and S, and the distribution

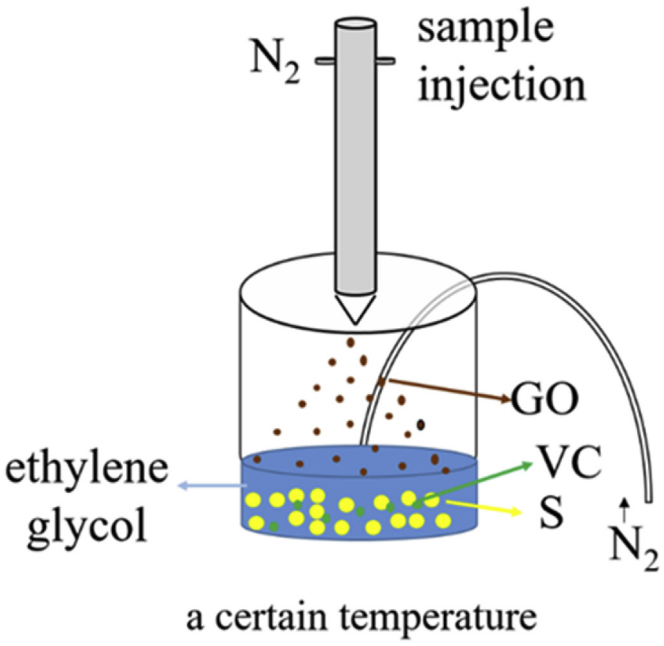

Fig. 1. Schematic for the synthesis of the S-prGO composites. (A colour version of this figure can be viewed online.)

of S on the surface of prGO, we use SEM to characterize the composite materials and the results are shown in Fig. 2. It is easy to see that uniform S-prGO composite materials can be obtained. As can be seen from Fig. 2b ~ 2d, S-prGO composite materials are comprised of wrinkle micro pieces with S evenly coated on their surfaces, and no separate large S particles were observed. As shown in Fig. 2e ~ g, the morphology of the composites did not change when combined with PDA.

In order to further observe the distribution of S on the surface of prGO, we used TEM for characterization, and the test results are shown in Fig. 3. From Fig. 3 we can see that S is symmetrically distributed on the surface of prGO in the form of nanoparticles without aggregation. The high resolution TEM of the electron beam has a higher energy which will cause the sublimation of S getting faster, but the result that we can still observed the existence of S NPs under high resolution TEM has demonstrated that there is a strong interaction between S and prGO.

The X-ray diffraction (XRD) of the S-prGO-PDA composites is shown in Fig. 4a. From Fig. 4a, all the XRD characteristic peaks of S-prGO-PDA composite materials are consistent with sublimation S, so that we can say that the crystal structure of S did not changed. The characteristic peaks of GO and prGO are not observed which further demonstrate that S is evenly coated on the surface of prGO. The thermogravimetric analysis of the S-prGO-PDA is shown in Fig. 4b. Fig. 4b shows that the S loading in the S-prGO-160-PDA, S-prGO-VC-160-PDA and S-rGO-VC-180-PDA composites are 79.3%, 58.1% and 69.1%, respectively. We have performed the elemental analysis to verify the TGA results of sulfur. The result obtained is shown in Table S1. The S loading in the S-prGO-160-PDA, S-prGO-VC-160-PDA and S-rGO-VC-180-PDA composites are 71.3%, 59.8% and 67.4%, respectively. The content of sulfur used in elemental analysis is slightly lower. The S-prGO composites were also analyzed by laser Raman spectroscopy. Fig. 5 shows the Raman

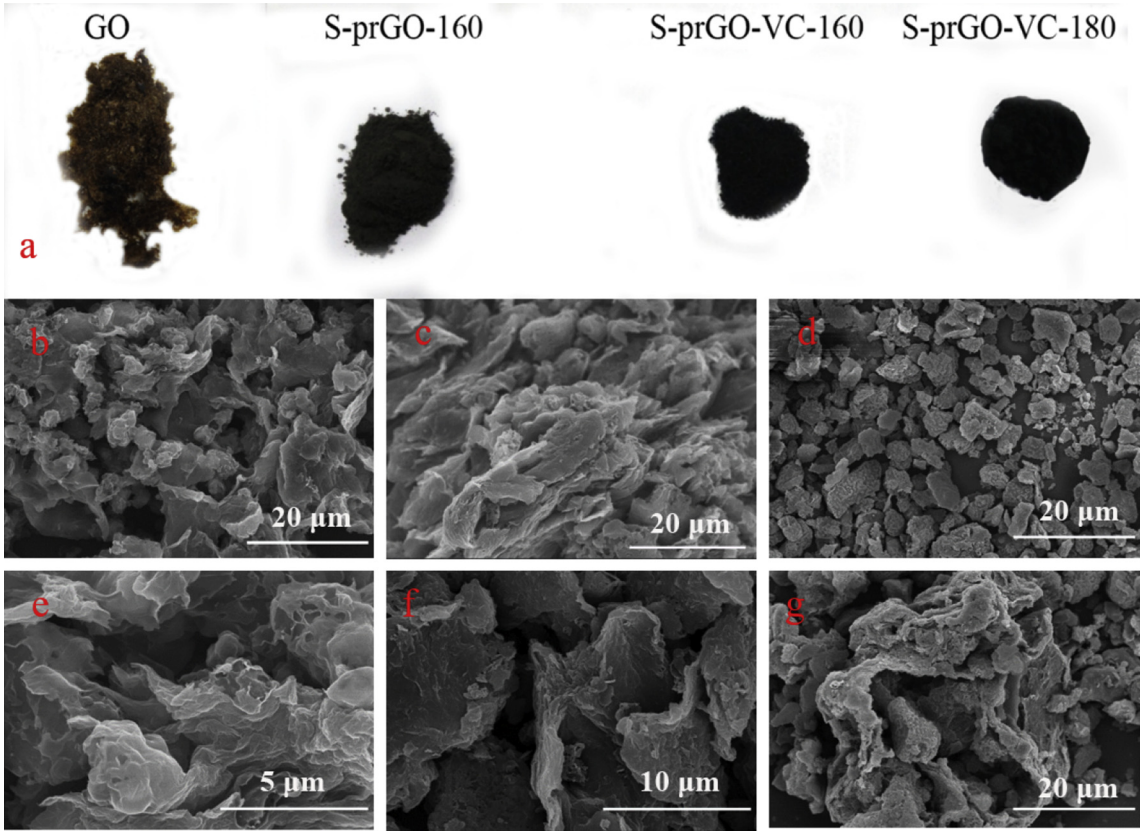

Fig. 2. (a) apparent photographs of the GO, S-prGO-160, S-prGO-VC-160 and S-prGO-VC-180. SEM images: (b) S-prGO-160, (c) S-prGO-VC-160, (d) S-prGO-VC-180, (e) S-prGO-160-PDA, (f) S-prGO-VC-160-PDA, (g) S-prGO-VC-180-PDA. (A colour version of this figure can be viewed online.)

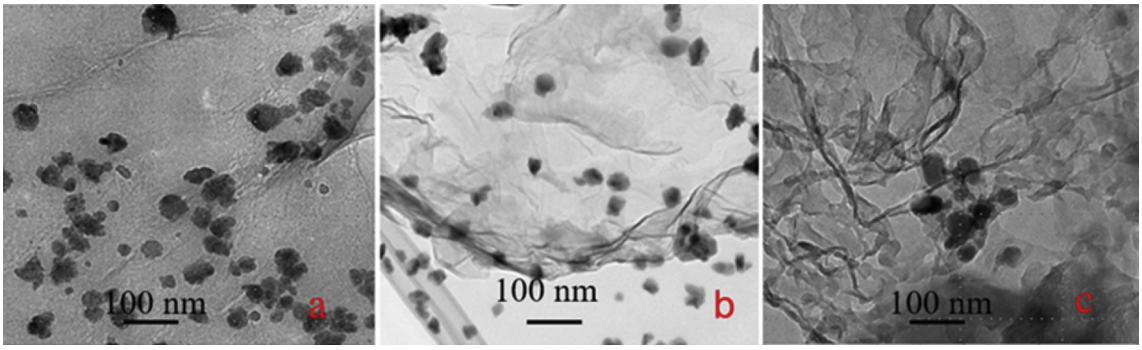

Fig. 3. TEM images: (a) S-prGO-160, (b) S-prGO-VC-160, (c) S-prGO-VC-180. (A colour version of this figure can be viewed online.)

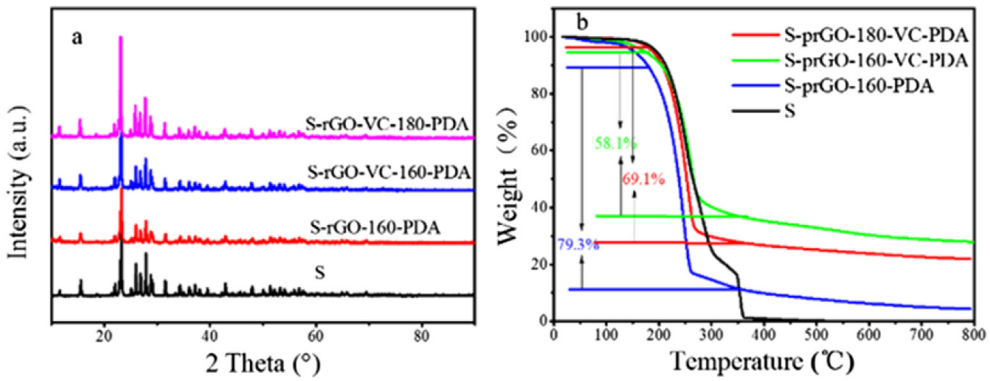

Fig. 4. (a) XRD patterns, (b) thermogravimetric analysis of the S-prGO-PDA. (A colour version of this figure can be viewed online.)

spectra of the S-prGO composites. As seen from Fig. 5a, the spectra of the S-prGO-160, S-prGO-VC-160 and S-rGO-VC-180 composites all have characteristic peaks of S, so that we can say that S has no changed under the process of preparation. The laser Raman spectroscopic analysis agrees well with the XRD data. And every curve has two major characteristic peaks at ~1350 cm^{-1} and ~1600 cm^{-1}, respectively. The G band at ~1600 cm^{-1} attributes to the vibration of *sp2* carbon atoms in a 2D hexagonal lattice and the D band at ~1350 cm^{-1} corresponds to the disorder and defects in the hexagonal graphitic layers [31–33]. From Fig. 5b, we can find that the ratio of I_D/I_G for S-prGO composites are gradually increased for GO, S-prGO-160, S-prGO-VC-160 and S-prGO-VC-180, successively. The increased I_D/I_G gives evidence that the reduction degree of graphene oxide gradually increases [13].

The S-prGO-PDA composites as the cathode material were assembled in CR-2016 coin type cells and their electrochemical performances were tested. Fig. 6a shows the initial galvanostatic discharge/charge profiles of the S-prGO-PDA composites at current density of 200 mA g^{-1}. All discharging curves show the high-potential plateau at ~2.3 V and the low-potential plateau (~2.1 V) with a tailing slope, which are consistent with the solid–liquid–solid transformation mechanism [34,35]. The S-prGO-VC-180-PDA composite exhibits greater overall specific capacity as well as greater capacity in discharge plateaus, suggesting better utilization of sulfur. At the same time, in contrast to the S-prGO-160-PDA and S-prGO-VC-160-PDA composites, the voltage gap between the charge plateau and the discharge plateau of the S-prGO-VC-180-PDA composite is smaller. Moreover, as shown in Fig. 6c,

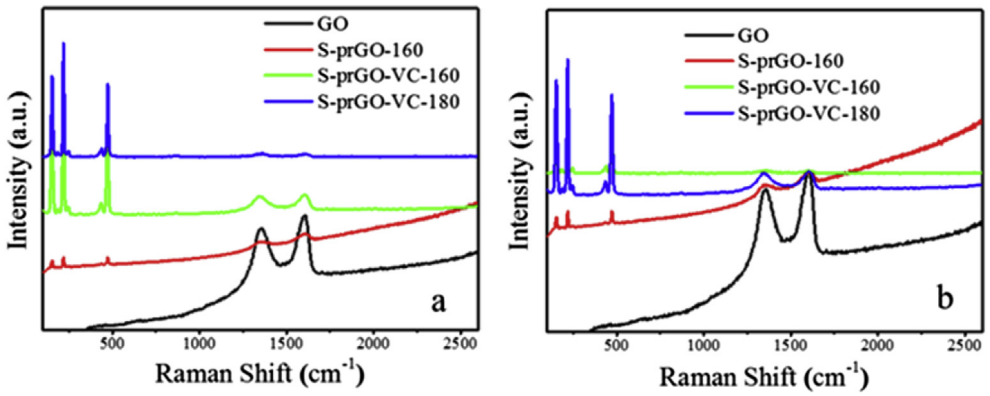

Fig. 5. Laser Raman spectra of the S-prGO. (a) unprocessed data, (b) obtained from dividing all the peak intensities of each curve in Figure (a) by the corresponding peak intensity of G. (A colour version of this figure can be viewed online.)

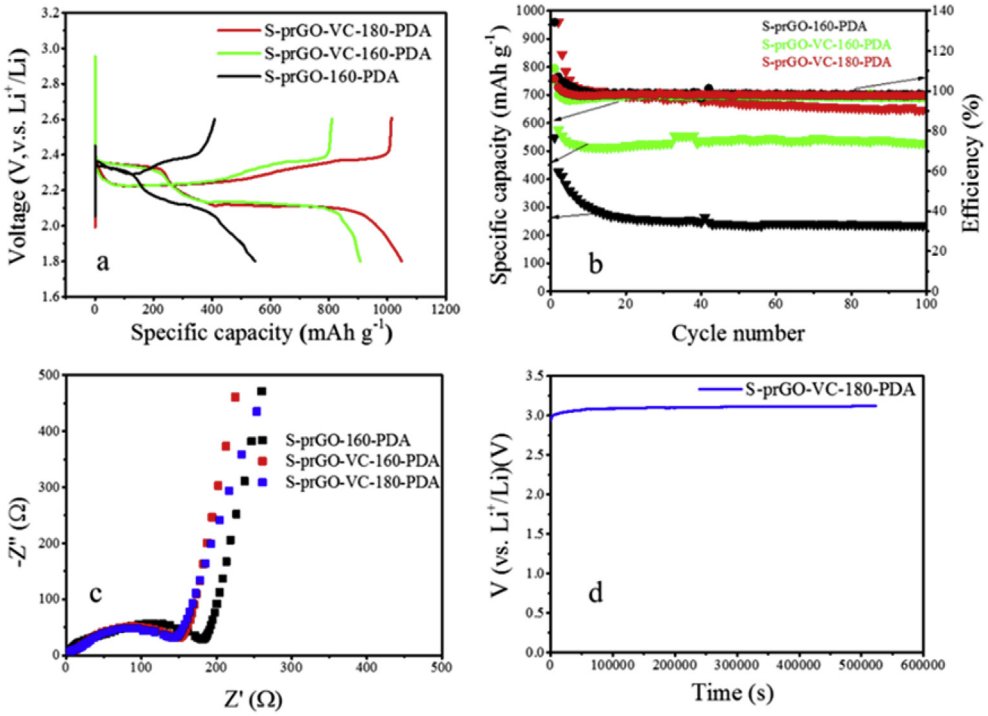

Fig. 6. Electrochemical performance of Li/(S-prGO-PDA) cells at a current density of 200 mA g-1. (a) discharge-charge profiles, (b) cycling performances, (c) EIS, (d) open circuit voltage. (A colour version of this figure can be viewed online.)

the EIS of all S-prGO-PDA composites shows a depressed semicircle in the high frequency region followed by an inclined line in the low frequency region. The charge transfer resistance, R_{ct}, obtained from the fitting results exhibits a significant and monotonic decrease as the reduction degree of prGO increases, which indicates faster kinetics in the S-prGO-VC-180-PDA composite [36,37]. Because the R_{ct} of as-prepared batteries mainly reflects the resistance of the electrode/electrolyte interface, the decrease of R_{ct} with the increasing reduction degree of prGO can be attributed to improved electrical contact between the prGO and small S NPs.

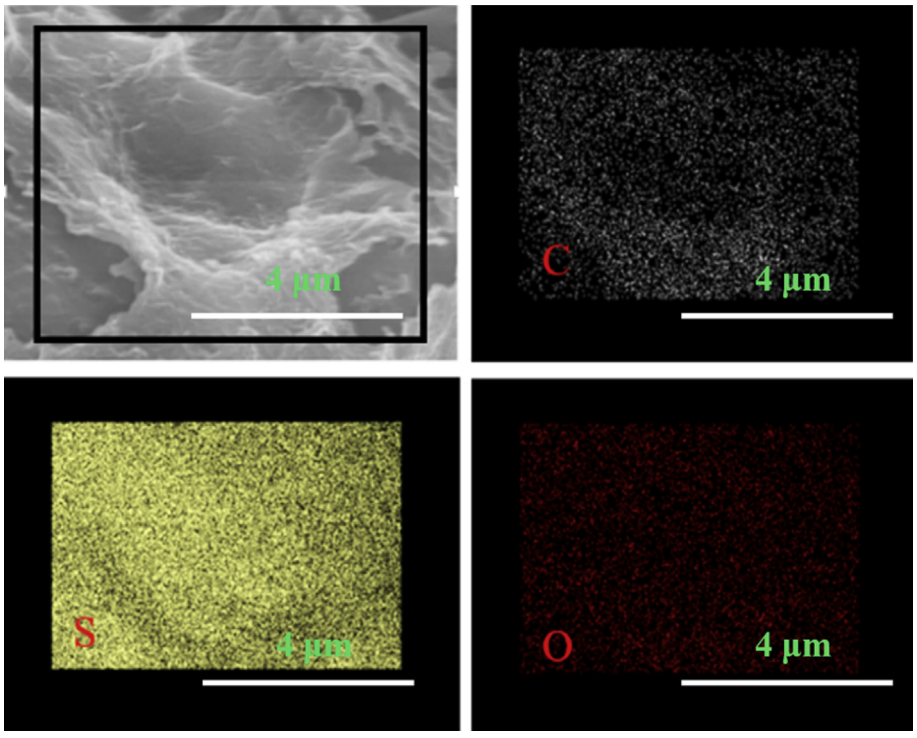

Fig. 7. Element mapping of the S-prGO-VC-180. (A colour version of this figure can be viewed online.)

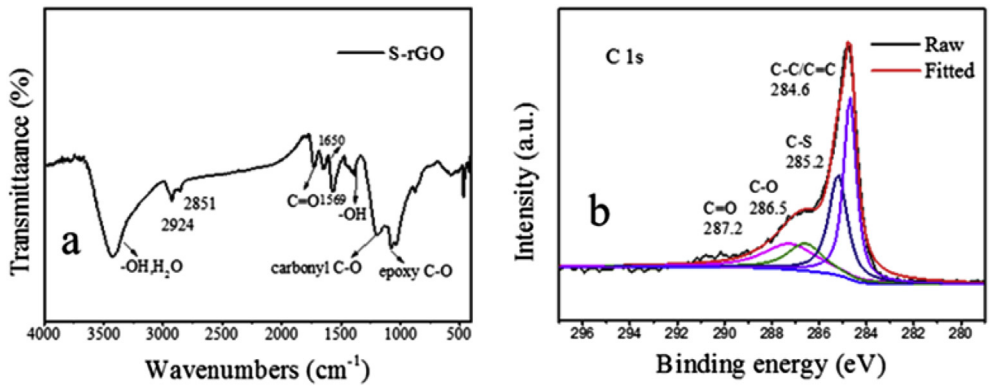

Fig. 8. (a) infrared spectrum of the S-prGO-VC-180, (b) XPS of the S-prGO-VC-180. (A colour version of this figure can be viewed online.)

The cycling performance of the S-prGO-PDA composites at current density of 200 mA g^{-1} is shown in Fig. 6b. These batteries show good cycle stability. After 100 cycles, the capacity can maintain 70%–80% of the initial capacity and coulombic efficiency approaches to 98%. The specific capacity of the S-prGO-VC-180-PDA composite is the highest among the S-prGO-160-PDA, S-prGO-VC-160-PDA and S-prGO-VC-180-PDA composites. The specific capacity of the S-prGO-VC-180-PDA composite is 1122 mAh g^{-1} at the first discharge and 647 mAh g^{-1} after 100 cycles. Following the electrochemical studies and long-term cycle capability testing of the S-prGO-VC-180-PDA, we next investigated the rate performance as shown in Fig. S1. The rate performance of the S-prGO-VC-180-PDA is relatively poor at the high charge-discharge rates. This is because that the electrical conductivity the partly reduced GO and the Li^+ conductivity of Li_2S are poor. We have compared the performance of the current composite cathode with other rGO based cathode for Li-S batteries, the results are shown in Table S2. As we can see from Table S2, our composite material exhibits good electrochemical properties. The improved cycling stability probably originates from restricted polysulfide diffusion due to the increase of specific contact area between prGO and S NPs, and the demonstrated strong sulfur adsorption effects of graphene-based materials derived from the high specific surface area [14]. In addition, the residual functional groups on prGO surface may also contribute to the immobilization of sulfur or polysulfides, and the amino groups of PDA can well fixed polysulfides. Both effects will help to alleviate the shuttle effect and improve the cycle stability [13]. However, it can be attributed to the improved electrical contact between the prGO and small S NPs with the increase of reduction degree of prGO, and, thereby, the increase of S utilization that the specific capacity of the S-prGO-PDA composites gradually improves.

In order to understand the excellent electrochemical properties of the S-prGO-VC-180-PDA composite material, we have carried out a series of researches. Fig. 6d and Fig. S2 show the variation of the open circuit voltage (OCV) of the S-prGO-VC-180-PDA with time at fresh status and after ten cycles. It's clearly to see that the OCV is stable, indicating a low self-discharge rate and good ability of fixed sulfur. The energy-dispersive X-ray spectroscopy (EDX) element mapping of S-prGO-VC-180 composite material fresh and after ten cycles are shown in Fig. 7 and Fig. S3. Fig. 7, at fresh status, further confirms the uniform distribution of S and O element on prGO surface. From Fig. S3, we can see that the S and O element are still uniformly distributed on prGO surface while a few S element distributed separately. This shows that a small part of S is not fixed in the charge-discharge process. Thus it explains the attenuation of specific capacity during the charge-discharge process. To further determine whether there are oxygen-containing functional groups in the S-prGO-VC-180-PDA composite material, namely whether the GO is fully restored, we used IR spectroscopy characterization for the S-prGO-VC-180 composite material, and the result is shown in Fig. 8a. As can be seen from the IR spectrum of the S-prGO-VC-180 composite material, the stretching vibration peaks assigned to the C═O, −OH, carbonyl C-O and epoxy −C−O still exist, indicating that the GO is just partly reduced. The stretching vibrations of CH_2 group are at 2924 cm^{-1} and 2851 cm^{-1}, the C═C stretching vibrations of aromatic ring are at 1569 cm^{-1} and 1650 cm^{-1}. The XPS was further used to detect what functional groups exist in the composite material and the result is shown in Fig. 8b. The peak at 284.6 eV belongs to carbon *sp2* hybridization, namely C-C or C═C, and the peaks at 286.5 eV and 287.2 eV are characteristic peaks of C-O and C═O, respectively. Although the two peaks are weak, it also proves that the S-prGO-VC-180 composite material also has certain oxygen-containing functional groups, reduction of GO is only partly, which are consistent with the above results. Simultaneously, for the S-prGO-VC-180 composite, the characteristic peak at 285.2 eV in XPS C1s spectrum, which is partially ascribed to the C-S bonds, indicating that there are certain chemical bonds between S and prGO in S-prGO-VC-180 composite. The XPS of GO, S-prGO-160 and S-prGO-VC-160 are shown in Fig. S4. As we can see from Fig. S4, the peaks 287.2 eV, 286.5 eV and 284.6 eV existed in GO, S-prGO-160 and S-prGO-VC-160, just similar to the peaks in S-prGO-VC-180, but the intensity of GO, S-prGO-160, S-prGO-VC-160 and S-prGO-VC-180 declined in order, which is consisting with Raman test results, indicating the reduction degree increased.

4. Conclusions

We have prepared the S-prGO composites by spray drying *in-situ* reduction method. Then, the S-prGO-PDA composites are obtained through the recombination of the S-prGO composites with PDA. S is evenly distributed on the surface of prGO in the form of nano-particles without aggregation. The S-prGO-PDA composite is a preferable host to fix S, resulting in a favorable electrochemical performance. The cycle performance, coulombic efficiency and capacity retention rate have been greatly improved. When charged-discharged at current density of 200 mA g^{-1} in the case of the S-prGO-PDA composite, the specific capacity is 1122 mAh g^{-1} at the first discharge and 647 mAh g^{-1} after 100 cycles, with stable coulombic efficiency of 98% for the Li/(S-prGO-PDA) cells. This work also demonstrates that control of the reduction degree of graphene oxide can adjust the ability of fixed sulfur and the conductivity of the S-prGO-PDA composite, leading to the significantly enhanced electrochemical performance.

Acknowledgments

We gratefully acknowledge the financial support of National Natural Science Foundation of China (Grant Nos. 21273185 and 21321062) and National Found for Fostering Talents of Basic Science (J1310024). The authors also wish to express their thanks to Prof. D. W. Liao for this valuable suggestions.

Appendix A. Supplementary data

Supplementary data related to this article can be found at http://dx.doi.org/10.1016/j.carbon.2016.11.079.

References

[1] X. Ji, K.T. Lee, L.F. Nazar, A highly ordered nanostructured carbon-sulphur cathode for lithium-sulphur batteries, Nat. Mater. 8 (2009) 500–506.
[2] X. Ji, S. Evers, R. Black, L.F. Nazar, Stabilizing lithium–sulphur cathodes using polysulphide reservoirs, Nat. Commun. 2 (2011) 325.
[3] A. Manthiram, Y.Z. Fu, Y.S. Su, Challenges and prospects of lithium-sulfur batteries, Acc. Chem. Res. 46 (2013) 1125–1134.
[4] H. Wang, Y. Yang, Y. Liang, J.T. Robinson, Y. Li, A. Jackson, et al., Graphene-Wrapped sulfur particles as a rechargeable lithium-sulfur battery cathode material with high capacity and cycling stability, Nano Lett. 11 (2011) 2644–2647.
[5] R.J. Chen, T. Zhao, F. Wu, From a historic review to horizons beyond: lithium-sulphur batteries run on the wheels, Chem. Commun. 51 (2015) 18–33.
[6] D. Fauteux, R. Koksbang, Rechargeable lithium battery anodes: alternatives to metallic lithium, J. Appl. Electrochem. 23 (1993) 1–10.
[7] M.M. Rao, W.S. Li, E.J. Cairns, Porous carbon-sulfur composite cathode for lithium/sulfur cells, Electrochem. Commun. 17 (2012) 1–5.
[8] J. Schuster, G. He, B. Mandlmeier, T. Yim, K.T. Lee, T. Bein, et al., Spherical ordered mesoporous carbon nanoparticles with high porosity for lithium-sulfur batteries, Angew. Chem. Int. Ed. 51 (2012) 3591–3595.
[9] N. Jayaprakash, J. Shen, S.S. Moganty, A. Corona, L.A. Archer, Porous hollow carbon@sulfur composites for high-power lithium-sulfur batteries, Angew. Chem. Int. Ed. 123 (2011) 6026–6030.
[10] S. Lu, Y. Cheng, X. Wu, J. Liu, Significantly improved long-cycle stability in high-rate Li–S batteries enabled by coaxial graphene wrapping over sulfur coated carbon nanofibers, Nano Lett. 13 (2013) 2485–2489.
[11] W.D. Zhou, H. Chen, Y.C. Yu, D.L. Wang, Z.M. Cui, F.J. Disalvo, et al., Amylopectin wrapped graphene oxide/sulfur for improved cyclability of lithium-sulfur battery, ACS Nano 7 (2013) 8801–8808.
[12] G. Zhou, L.C. Yin, D.W. Wang, L. Li, S. Pei, F. Li, et al., Fibrous hybrid of graphene and sulfur nanocrystals for high performance lithium–sulfur batteries, ACS Nano 7 (2013) 5367–5375.
[13] L. Ji, M. Rao, L. Zhang, Y. Li, W. Duan, J. Guo, et al., Graphene oxide as a sulfur immobilizer in high performance lithium/sulfur cells, J. Am. Chem. Soc. 133 (2011) 18522–18525.
[14] N. Li, M. Zheng, H. Lu, Z. Hu, C. Shen, X. Chang, et al., High-rate lithium-sulfur batteries promoted by reduced graphene oxide coating, Chem. Commun. 48 (2012) 4106–4108.
[15] J.L. Shi, H.J. Peng, L. Zhu, W. Zhu, Q. Zhang, Template growth of porous graphene microspheres on layered double oxide catalysts and their applications in lithium–sulfur batteries, Carbon 92 (2015) 96–105.
[16] C. Wang, W. Wan, J.T. Chen, H.H. Zhou, X.X. Zhang, L.X. Yuan, et al., Dual core–shell structured sulfur cathode composite synthesized by a one-pot route for lithium sulfur batteries, J. Mater. Chem. A 1 (2013) 1716–1723.
[17] F. Wu, J.Z. Chen, L. Li, T. Zhao, R.J. Chen, Improvement of rate and cycle performence by rapid polyaniline coating of a MWCNT/sulfur cathode, J. Phys. Chem. C 115 (2011) 24411–24417.
[18] L.X. Yuan, H.P. Yuan, X.P. Qiu, L.Q. Chen, W.T. Zhu, Improvement of cycle property of sulfur-coated multi-walled carbon nanotubes composite cathode for lithium/sulfur batteries, J. Power Sources 189 (2009) 1141–1146.
[19] S. Xin, L. Gu, N.H. Zhao, Y.X. Yin, L.J. Zhou, Y.G. Guo, et al., Smaller sulfur molecules promise better lithium-sulfur batteries, J. Am. Chem. Soc. 134 (2012) 18510–18513.
[20] J. Guo, Y. Xu, C. Wang, Sulfur-impregnated disordered carbon nanotubes cathode for lithium-sulfur batteries, Nano Lett. 11 (2011) 4288–4294.
[21] G.M. Zhou, D.W. Wang, F. Li, P.X. Hou, L.C. Yin, C. Liu, et al., A flexible nanostructured sulphur-carbon nanotube cathode with high rate performance for Li-S batteries, Energy Environ. Sci. 5 (2012) 8901–8906.
[22] W. Kong, L. Sun, Y. Wu, K. Jiang, Q. Li, J. Wang, et al., Binder-free polymer encapsulated sulfurecarbon nanotube composite cathodes for high performance lithium batteries, Carbon 96 (2016) 1053–1059.
[23] Y. Diao, K. Xie, S.Z. Xiong, X.B. Hong, Analysis of polysulfide dissolved in electrolyte in discharge-charge process of Li-S battery, J. Electrochem. Soc. 159 (2012) A421–A425.
[24] J. Nelson, S. Misra, Y. Yang, A. Jackson, Y.J. Liu, H.L. Wang, et al., In operando X-ray diffraction and transmission X-ray microscopy of lithium sulfur batteries, J. Am. Chem. Soc. 134 (2012) 6337–6343.
[25] Z. Li, H.B. Wu, X.W. Lou, Rational designs and engineering of hollow micro-/nanostructures as sulfur hosts for advanced lithium–sulfur batteries, Energy Environ. Sci. 9 (2016) 3061–3070.
[26] X.F. Wang, Z.X. Wang, L.Q. Chen, Reduced graphene oxide film as a shuttle-inhibiting interlayer in a lithium-sulfur battery, J. Power Sources 242 (2013) 65–69.
[27] G. Zheng, Q. Zhang, J.J. Cha, Y. Yang, W. Li, Z.W. Seh, et al., Amphiphilic surface modification of hollow carbon nanofibers for improved cycle life of lithium sulfur batteries, Nano Lett. 13 (2013) 1265–1270.
[28] Z.Y. Wang, Y.F. Dong, H.J. Li, Z.B. Zhao, H.B. Wu, C. Hao, et al., Enhancing lithium-sulphur battery performance by strongly binding the discharge products on amino-functionalized reduced graphene oxide, Nat. Commun. 5 (2014).
[29] Z. Li, J.T. Zhang, Y.M. Chen, J. Li, X.W. Lou, Pie-like electrode design for high-energy density lithium-sulfur batteries, Nat. Commun. 6 (2015) 8850.
[30] H.W. Chen, C.H. Wang, W.L. Dong, W. Lu, Z.L. Du, L.W. Chen, Monodispersed sulfur nanoparticles for lithium-sulfur batteries with theoretical performance, Nano Lett. 15 (2015) 798–802.
[31] J. Bai, X.E. Jiang, A facile one-pot synthesis of copper sulfide-decorated reduced graphene oxide composites for enhanced detecting of H_2O_2 in biological environments, Anal. Chem. 85 (2013) 8095–8101.
[32] Y.W. Zhang, J.Q. Tian, H.Y. Li, L. Wang, X.Y. Qin, A.M. Asiri, et al., Biomolecule-assisted, environmentally friendly, one-pot synthesis of CuS/reduced graphene oxide nanocomposites with enhanced photocatalytic performance, Langmuir 28 (2012) 12893–12900.
[33] X.J. Zhang, G.S. Wang, Y.Z. Wei, L. Guo, M.S. Cao, Polymer-composite with high dielectric constant and enhanced absorption properties based on graphene-CuS nanocomposites and polyvinylidene fluoride, J. Mater. Chem. A 1 (2013) 12115–12122.
[34] S.S. Zhang, Liquid electrolyte lithium/sulfur battery: fundamental chemistry, problems, and solutions, J. Power Sources 231 (2013) 153–162.
[35] S.S. Zhang, D.T. Tran, A proof-of-concept lithium/sulfur liquid battery with exceptionally high capacity density, J. Power Sources 211 (2012) 169–172.
[36] W. Li, Q. Zhang, G. Zheng, Z.W. Seh, H. Yao, Y. Cui, Understanding the role of different conductive polymers in improving the nanostructured sulfur cathode performance, Nano Lett. 13 (2013) 5534–5540.
[37] Z.F. Deng, Z.A. Zhang, Y.Q. Lai, J. Liu, J. Li, Y.J. Liu, Electrochemical impedance spectroscopy study of a lithium/sulfur battery: modeling and analysis of capacity fading, J. Electrochem. Soc. 160 (2013) A553–A558.